Available online at www.sciencedirect.com

jmr&t Journal of Materials Research and Technology

https://www.journals.elsevier.com/journal-of-materials-research-and-technology

Original Article

Synergistic interactions between wear and corrosion of Ti-16Mo orthopedic alloy

Wei Xu[a,b,1], Aihua Yu[a,1], Xin Lu[a,*], Maryam Tamaddon[b], Liqi Ng[b], Muhammad dilawer Hayat[c], Mengdi Wang[d], Jianliang Zhang[e], Xuanhui Qu[a], Chaozong Liu[b]

[a] Beijing Advanced Innovation Center for Materials Genome Engineering, State Key Laboratory for Advanced Metals and Materials, Institute for Advanced Materials and Technology, University of Science and Technology Beijing, Beijing, China
[b] Institute of Orthopaedic & Musculoskeletal Science, University College London, Royal National Orthopaedic Hospital, Stanmore HA7 4LP, UK
[c] Department of Chemical and Materials Engineering, University of Auckland, Auckland 1142, New Zealand
[d] School of Physiology, Pharmacology and Neuroscience, University of Bristol, Bristol BS8 1TD, UK
[e] School of Metallurgical and Ecological Engineering, University of Science and Technology Beijing, Beijing 100083, China

ARTICLE INFO

Article history:
Received 23 April 2020
Accepted 30 June 2020

Keywords:
Ti-16Mo alloy
Corrosion
Wear
Tribocorrosion
Orthopedic implant materials

ABSTRACT

In this study, corrosion, wear, and tribocorrosion of Ti-16Mo alloy manufactured by powder metallurgy (PM) in phosphate-buffered saline are investigated. The results indicate that the corrosion rate of Ti-16Mo alloy increases about 100 times from 0.00009 mm/yr to 0.00851 mm/yr under the tribocorrosion condition. Also, corrosion accelerates wear loss, and wear increment rate due to the corrosion (4.7715 mm/yr) of Ti-16Mo alloy is about 40% of pure mechanical wear rate (11.78 mm/yr). Compared with as-cast pure Ti (23.70999 mm/yr) and Ti-6Al-4 V (17.12003 mm/yr), Ti-16Mo alloy exhibits the lowest materials loss of 16.56001 mm/yr making it become a promising alloy for bone-tissue applications.

1. Introduction

Replacement of functional disordered hard tissues, e.g. hip joints and dental roots, with artificial instruments is becoming increasingly popular [1,2]. Currently, Titanium (Ti) and its alloys, such as commercial pure Ti (CP-Ti), Ti-6Al-4 V (Ti64) and Ti-5Al-2.5Fe alloys (wt.%, the composition of all alloy is presented by weight ratio hereafter), are widely used as the hard tissue implant alloys [3–6]. However, these alloys have several disadvantages. Firstly, CP-Ti possesses moderate strength and wear properties while Ti64 and Ti-5Al-2.5Fe alloys contain toxic vanadium (V) or aluminum (Al), which can lead to mental disorder and Alzheimer's disease [7]. Secondly, elastic modulus of CP-Ti (~110 GPa), Ti64, and Ti-5Al-2.5Fe (~120 GPa) is higher than the elastic modulus of human bone (0.01–30 GPa).

* Corresponding author.
E-mail: luxin@ustb.edu.cn (X. Lu).
[1] These authors contributed equally.

https://doi.org/10.1016/j.jmrt.2020.06.095

A mismatch in elastic modulus between them can cause stress shielding effect, which results in bone degeneration and eventually to failure [8]. Therefore, novel Ti alloys with lower elastic modulus and higher biocompatibility are needed urgently. Ti-Mo alloys have attracted increasing attention in recent years [9–14]. Compared with other Ti alloys, Ti-Mo alloys have servals advantages, as follows:

(1) Mo can lower the elastic modulus effectively by forming β-phase;
(2) Mo is a biocompatible element, and is nontoxic and non-allergenic;
(3) Mo has low magnetic susceptibility, which is beneficial for magnetic resonance imaging (MRI) diagnosis;
(4) Mo can increase strength and wear resistance through solution strengthening;
(5) The price of Mo is lower than the other widely used β-phase stabilizing elements, such as Niobium (Nb) and Zirconium (Zr).

Our previous study has demonstrated that Ti-16Mo alloy exhibited improved hardness, wear, and corrosion resistance with lower elastic modulus [15]. Then, Ti-16Mo alloy is selected for this study.

Corrosion and wear properties are the two important factors that affect the life span of alloys. At present, corrosion and wear behaviors of Ti-Mo alloys are usually studied separately as isolated systems [16,17]. But implants are generally encompassed by body fluids in the human body that induces corrosion. Also, there is relative motion between the implant and bone as well, such as sliding and fretting. Therefore, wear and corrosion can occur simultaneously when the alloys are implanted into the human body. This simultaneous occurrence phenomenon is called tribocorrosion [18,19]. It is usually irreparable and happens on the surface of the implant [20,21]. Under tribocorrosion, the deterioration of the alloy is exacerbated and much larger than the sum of the material loss by corrosion and wear alone. Hence, systematic studies about the synergistic interactions between wear and corrosion behaviors of Ti-Mo alloy are vital but still scarce in the literature.

In the present study, the wear, corrosion, and synergistic interactions between them (tribocorrosion) of Ti-16Mo alloy were investigated. This study aims to establish a basic understanding of Ti-16Mo alloy degradation in terms of pure corrosion, pure mechanical wear, and tribocorrosion. It also aims to provide some insights into the interaction mechanisms between pure mechanical wear and corrosion of Ti-16Mo alloy, which will provide basic supports for its practical application as hard-tissue implant materials.

2. Materials and methods

2.1. Specimen preparation

Ti-16Mo alloy was manufactured through the powder metallurgy (PM) using commercial Ti and Mo powders. The size of Ti powder is $\leq 45\ \mu m$ while the size of Mo powders is $\leq 25\ \mu m$. All powders have a purity of 99.9%. The powders are mixed firstly and then pressed into a cylinder. Finally, the cylinder was sintered under the Ar atmosphere at 1500 °C for 2 h. The detailed sintering procedure, particle size, and impurity content can be found elsewhere [22–26].

2.2. Tribocorrosion and pure mechanical wear tests

The tribocorrosion of Ti-16Mo was investigated in phosphate-buffered saline (PBS) by a ball-on-plate-tribometer (UMT-II) at 37 ± 0.5 °C. The tribometer was integrated with an electrochemical workstation to monitor the corrosion behavior during sliding. Rectangular plates (20 mm × 6 mm × 2 mm) were cut by electrical discharge machining (EDM). Then specimens were then ground to 2000 grits by SiC abrasive paper and followed by mechanical polished. Commercial cast CP-Ti and Ti64 alloys were tested simultaneously as references. The slip frequency was 1 Hz, and the corresponding slip speed was 0.03 m/s. The stroke lengths were 15 mm. The applied load was 1.5 N, which lead to a Hertzian contact pressure of 315−325 MPa for all three alloys. The counter material was ZrO_2 ball, which has a high hardness of 700 HV, and the diameter was 10 mm. Also, to obtain the pure wear rate, the tribocorrosion measurement was also performed under a potential of -0.8 V (vs. SCE), namely pure mechanical wear. The coefficient of friction (COF) and open circuit potential (OCP) before, during, and after sliding were recorded. For tribocorrosion and pure mechanical wear tests, 5 experiments were repeated to verify the reproducibility, and the results were expressed as mean ± standard deviation (SD).

2.3. Electrochemical test

Potentiodynamic polarization (PD) measurements with and without sliding were measured by a three-electrode electrochemical workstation based on the ASTM G59-97 standard [27]. The size of the test samples is the same as the samples used in tribocorrosion and pure mechanical wear tests. Epoxy resin was used to seal the samples, and the exposed area was 120 mm^2. Before the PD measurements, all samples were ground with 2000 grit SiC abrasive paper and immersed into the PBS solution for 2 h to stable the potential of samples. The scan rate was 0.5 mV/s while the scan rate was -0.3−2 V vs OCP. The corrosion potential (E_{corr}) and corrosion current density (I_{corr}) were obtained from PD curves. For the electrochemical test, 5 experiments were repeated to verify the reproducibility, and the results were expressed as mean ± standard deviation (SD).

2.4. Characterization

X-ray diffractometer was used to investigate the phase constituents of the alloys. The target and wavelength were copper (Cu) and 0.15406 nm, respectively. Micro-hardness was tested by a Buehler Micromet 2100 tester based on the ASTM E384-11 standard [28], and the load was 0.5 N. The topography and chemical composition of all samples after tribocorrosion and wear tests were examined by an SEM (JSM-6480LV, Japan) integrated with an energy dispersive X-ray spectrometry (EDS). A white light interference microscope was used to observed the profile of the wear tracks after tribocorrosion and wear tests.

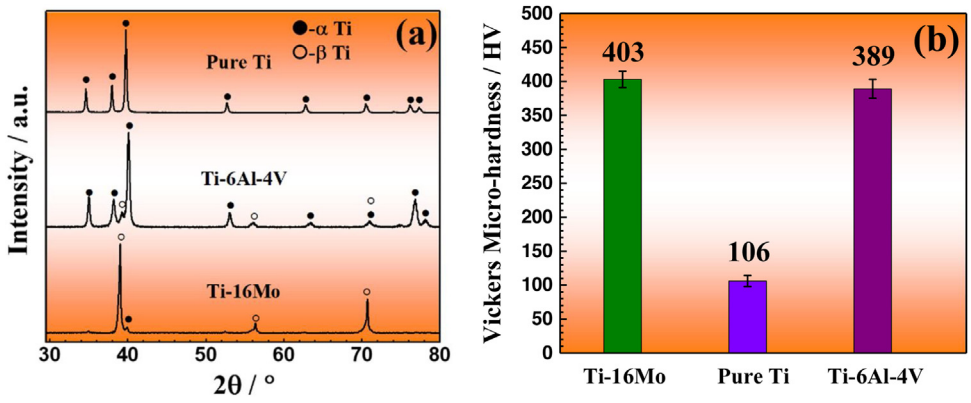

Fig. 1 – (a) XRD and (b) Vickers micro-hardness of Ti-16Mo, as-cast CP-Ti and Ti64 alloys.

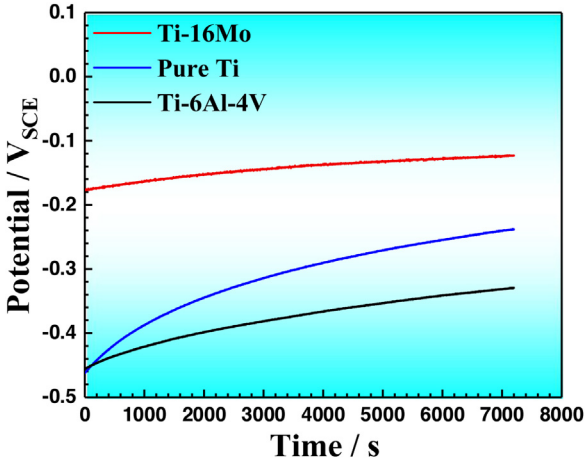

Fig. 2 – OCP vs. time for Ti-16Mo, as-cast CP-Ti and Ti64 alloys before static corrosion test in PBS solution at 37 ± 0.5 °C.

The material's loss was calculated based on the profile of the wear tracks.

2.5. *Quantitative calculation*

Total materials loss rate under wear and corrosion (T, mm/yr) and pure wear rate (W_0, mm/yr) were calculated according to ASTM G119-09 [29]:

$$W = \frac{\Delta m}{S \times \rho \times t} \times 24 \left(\frac{h}{d}\right) \times 365 \left(\frac{d}{y}\right) \quad (1)$$

where, Δm is the wear loss, which was calculated indirectly from the white light interference microscope, g; ρ is specimen density, g/cm^3; S is the area of worn surface, mm^2; t is test time, h.

The pure corrosion rate (C_0, mm/yr) and corrosion rate with wear (C_W, mm/yr) can be obtained from the following equation:

$$C = K \times \left(\frac{I_{corr}}{\rho}\right) \times EW \quad (2)$$

where, C is the corrosion rate, mm/yr, K is 3.27×10^{-3}, mm g/μA·cm·y; ρ is the density, g/cm^3; I_{corr} is the corrosion current density, A/cm^2; EW is the equivalent weight, 12.5 for Ti-16Mo, 11.9 for CP-Ti and 12.01 for Ti64, respectively.

Based on T and C_W, the wear rate with corrosion (W_C, mm/yr) can be calculated by the formula (3):

$$W_C = T - C_W \quad (3)$$

By combining W_0 and C_0, ΔW_C (wear increment due to the corrosion, mm/yr) and ΔC_W (corrosion increment due to the wear, mm/yr) can be obtained based on the Eq.s (4) and (5):

$$\Delta W_C = W_C - W_0 \quad (4)$$

$$\Delta C_W = C_W - C_0 \quad (5)$$

3. Results and discussion

3.1. *Structural characterization and Vickers micro-hardness*

Fig. 1 shows Vickers micro-hardness and XRD patterns of Ti-16Mo, CP-Ti, and Ti64 alloys. As shown in Fig. 1(a), The Ti-16Mo alloy is characterized by the β phase with a small amount of α phase while the CP-Ti and Ti64 alloys consist of α phase and α + β phases, respectively. The Ti-16Mo alloy exhibits the highest hardness of 403 HV, which is significantly higher than that of CP-Ti (106 HV) and even higher than that of Ti64 alloy (389 HV) (Fig. 1(b)). The highest hardness of Ti-16Mo among three alloys is due to Mo added. Mo is a strong solid solution element, and its addition to Ti alloys can significantly improve the strength [8,30].

3.2. *Electrochemical behavior*

3.2.1. OCP

Fig. 2 shows the OCP evaluation of all three alloys during 2 h immersion before the static corrosion test. All the curves exhibit similar variations. The E_{OCP} shifts in a positive direction as the immersion time increases and reaches a quasi-stationary value after immersion for 2 h. Ti-16Mo alloy

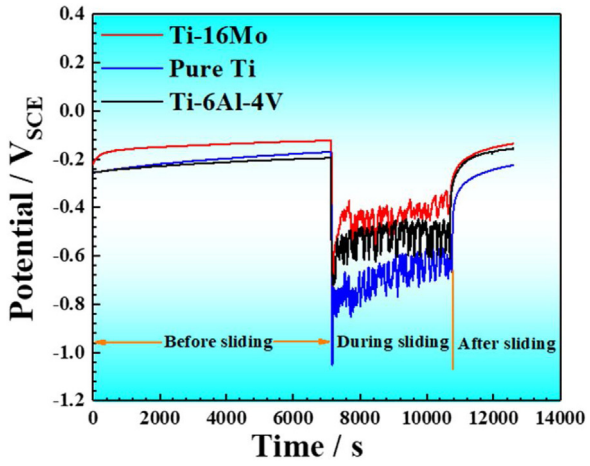

Fig. 3 – OCP vs. time for Ti-16Mo, as-cast CP-Ti and Ti64 alloys before, during, and after sliding in PBS solution at 37 ± 0.5 °C.

presents nobler potential (-0.125 V) compared with CP-Ti (-0.238 V) and Ti64 (-0.332 V) alloys.

Variation of OCP during tribocorrosion is presented in Fig. 3. Similar to the OCP before the static corrosion test, the OCP before sliding increases gradually, and reaches a final quasi-stationary state-stage after some time. When sliding starts, the OCP falls abruptly. After a few minutes, the OCP reaches a steady state. In general, OCP is a mixed potential of active areas and passive unworn areas, and it is affected by the ratio of these two areas [31]. It should be noted that before sliding the surface of all samples formed stable oxide films. When sliding started the formed mixed oxide films were damaged by the mechanical action at the contact region [32,33], leading to a sharp decrease in OCP. However, when the depassivation and passivation rates reached a dynamic equilibrium, all the samples exhibited a steady potential. Compared with the potential of CP-Ti (−0.664 V) and Ti64 (−0.507 V) alloys, the Ti-16Mo alloy exhibits a much nobler potential of -0.431 V during sliding. After sliding the OCP of all three alloys gradually attain the pre-sliding values, indicating repassivation behavior occurred [34]. Among the three alloys, the Ti-16Mo alloy exhibits the highest potential of −0.136 V after sliding, meaning that the Ti-16Mo alloy has the highest repassivation capability.

3.2.2. *Potentiodynamic polarisation*

PD curves of Ti-16Mo, CP-Ti, and Ti64 alloys in PBS solution at 37 ± 0.5 °C under static corrosion and tribocorrosion conditions are shown in Fig. 4. It can be found that there is no significant difference for all of the cathodic branches, indicating there is a similar cathodic reaction occurred. The anodic branches under both static corrosion and tribocorrosion conditions also exhibit similar curves, chartered by three potential domains. Take Ti-16Mo alloy under static corrosion for example (Fig. 4(a)), the first potential domain is between −0.22 V (E_{corr}) and −0.25 V, which current density rises with scanning potential until it reaches the second potential domain (0.25–1.1 V). When the scanning potential exceeds 1.1 V, it enters the third potential domain, where the current density increases with the scanning potential again, this time because of the destruction of the formed oxide film by the high overpotential. Under tribocorrosion (Fig. 4(b)), E_{corr} of all alloys shifts to a negative potential, and the corrosion current density (I_{corr}) decreases significantly, indicating that accelerated corrosion is induced by mechanical wear.

Table 1 shows E_{corr} and I_{corr} obtained from PD polarization curves. As Table 1 shown, compared with the values under static corrosion, the E_{corr} of all three alloys shifts to negative about 200 mV, and the I_{corr} increases by approximately two orders of magnitude under tribocorrosion. The corrosion rates calculated by Eq. (2) are also shown in Table 1. Similar to the results of I_{corr}, the corrosion rate of all three alloys increases under tribocorrosion. Among three alloys, the Ti-16Mo alloy presents the noblest potential and the lowest corrosion rate under both static corrosion and tribocorrosion, meaning that Ti-16Mo has the highest corrosion resistance.

3.3. *Wear behavior*

Fig. 5 shows COF of Ti-16Mo, CP-Ti, and Ti64 alloys under pure mechanical wear and tribocorrosion. COF of all three alloys is higher in tribocorrosion conditions than for pure mechanical wear conditions. Under tribocorrosion, the surface layer gets corroded increasing the frictional forces, which leads to stringer friction [35]. The Ti-16Mo alloy presents the lowest

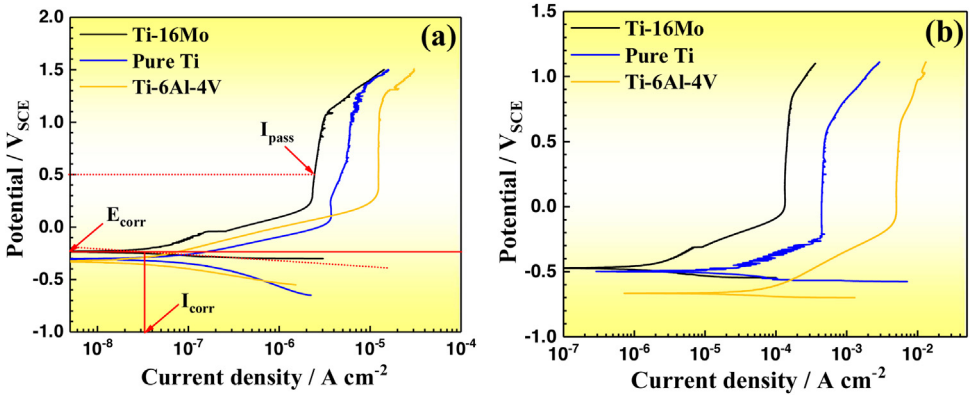

Fig. 4 – PD curves of Ti-16Mo, as-cast CP-Ti, and Ti64 alloys in PBS solution at 37 ± 0.5 °C measured under static corrosion (a) and trribocorrosion (b).

Table 1 – Extracted corrosion parameters from PD curves for Ti-16Mo, as-cast CP-Ti, and Ti64 alloys in naturally aerated PBS solution at 37 ± 0.5 °C.

	Static corrosion			Tribocorrosion		
Alloy	E_{corr} (V)	$I_{corr} \times 10^{-8}$ (A/cm^2)	$C_0 \times 10^{-4}$ (mm/yr)	E_{corr} (V)	$I_{corr} \times 10^{-6}$ (A/cm^2)	$C_W \times 10^{-2}$ (mm/yr)
Ti-16Mo	−0.234 ± 0.05	1.02 ± 0.15	0.912 ± 0.09	−0.474 ± 0.05	1.03 ± 0.13	0.851 ± 0.07
CP-Ti	−0.301 ± 0.06	3.77 ± 0.16	3.221 ± 0.15	−0.498 ± 0.15	4.48 ± 0.21	3.862 ± 0.11
Ti64	−0.329 ± 0.08	6.72 ± 0.19	6.114 ± 0.21	−0.663 ± 0.21	7.93 ± 0.19	7.123 ± 0.19

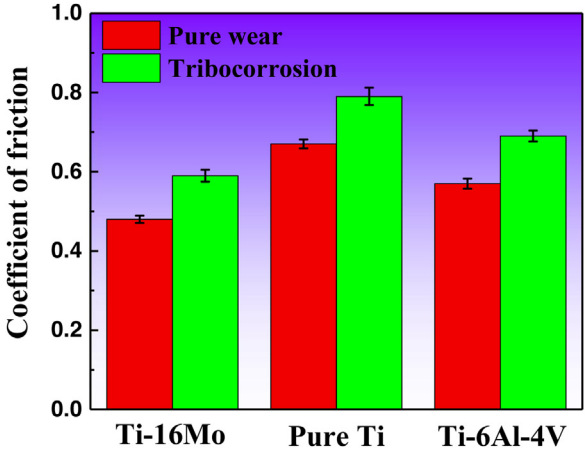

Fig. 5 – COF of Ti-16Mo, as-cast CP-Ti and Ti64 alloys in PBS solution at 37 ± 0.5 °C under pure mechanical wear and tribocorrosion condition.

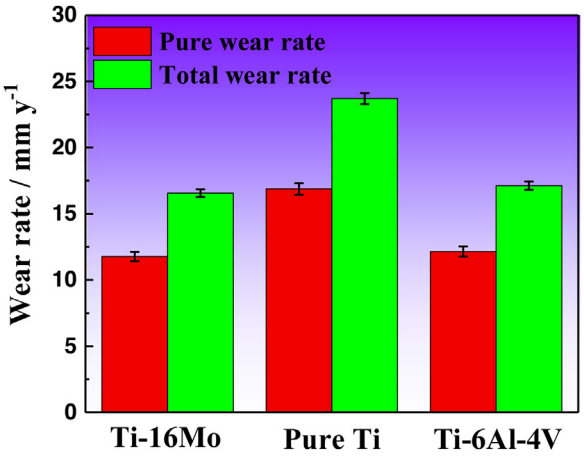

Fig. 7 – Wear rate of Ti-16Mo, as-cast CP-Ti and Ti64 alloys in PBS solution at 37 ± 0.5 °C under pure mechanical wear and tribocorrosion test conditions.

average COF under pure mechanical wear (0.48) and tribocorrosion conditions (0.59), much lower than those of CP-Ti (0.67 and 0.79) and Ti64 alloy (0.57 and 0.69), respectively.

Wear tracks recorded on Ti-16Mo alloy, CP-Ti, and Ti64 after the tribocorrosion and pure mechanical wear test are presented in Fig. 6. Similar to the results of COF, wear tracks under the tribocorrosion condition are wide and deep for all the three alloys. Among three alloys, Ti-16Mo alloy exhibited the narrowest wear track of 0.948 mm and 0.332 mm under tribocorrosion and pure mechanical wear conditions, respectively, suggesting that the Ti-16Mo alloys have a greater wear resistance than CP-Ti and Ti64 alloy.

Calculated wear rate after the tribocorrosion and pure mechanical wear test is shown in Fig. 7. The wear rates of Ti-16Mo, CP-Ti, and Ti64 alloys under tribocroosion conditions are 16.56 mm/yr, 23.71 mm/yr, and 17.12 mm/yr, respectively, while under pure mechanical conditions is 11.78 mm/yr, 16.88 mm/yr, and 12.16 mm/yr. Under tribocorrosion conditions, the wear material loss has roughly increased by about 40%. This is mainly because the fact that the fresh metal underneath exposed due to the passive film formed on the surface is peeled off can be corroded, which ultimately accelerates the wear loss [36]. Ti-16Mo alloy, however, exhibits the lowest wear rate irrespective of the conditions.

Fig. 8 shows the surface morphology of all alloys after tribocorrosion and pure mechanical wear tests. It can be found that parallel grooves are existed to the sliding direction for alloys under both tribocorrosion and pure mechanical wear tests, suggesting that an abrasive wear mechanism occurs. Besides, two different zones (dark and grey) can be found in the BSE-SE

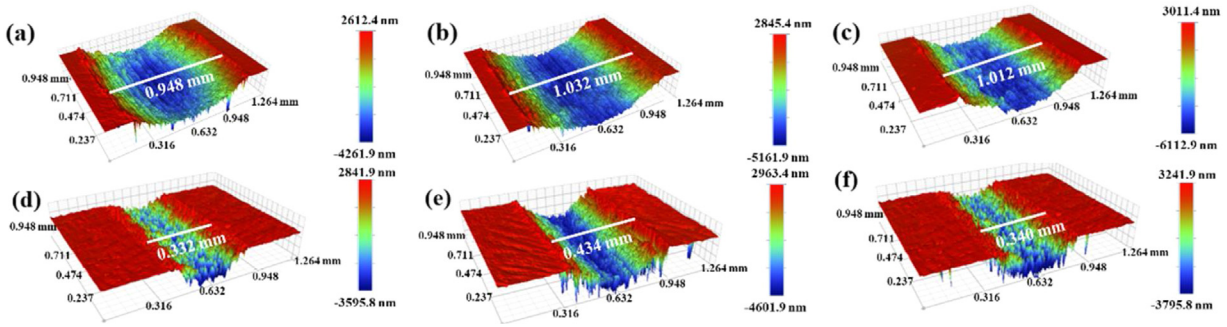

Fig. 6 – 3D surface profilometry recorded on Ti-16Mo, as-cast CP-Ti and Ti64 alloys after tribocorrosion test (a-c) and pure wear test (d-f) at 37 ± 0.5 °C: (a), (d) Ti-16Mo alloy; (b), (e) CP-Ti; (c), (f) Ti64.

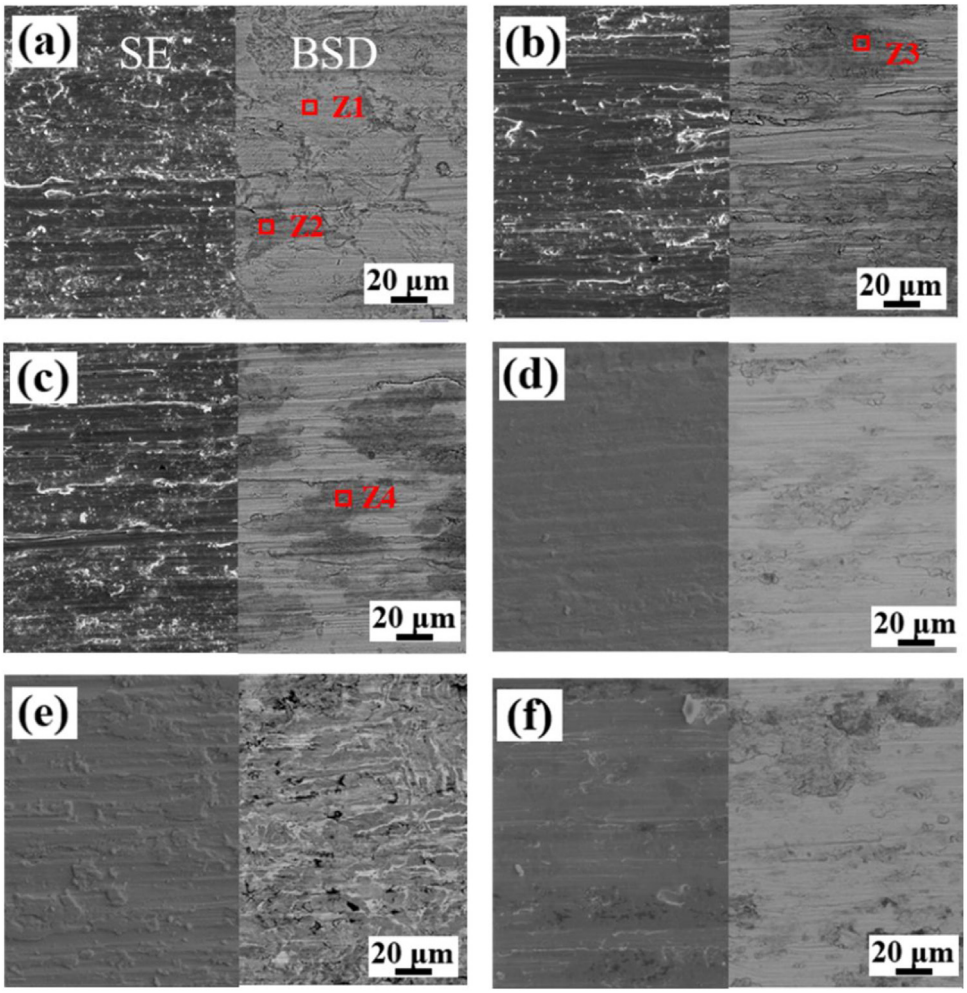

Fig. 8 – Detailed back-scattered electron and secondary electron (BSE-SE) images of the worn surfaces after tribocorrosion test (a-c) and pure wear test (d-f) at 37 ± 0.5 °C: (a), (d) Ti-16Mo alloy; (b), (e) CP-Ti; (c), (f) Ti64.

images under both tribocorrosion and pure mechanical wear conditions. To identify the chemical of these two zones, EDS was carried out. Taking Ti-16Mo alloy under tribocorrosion for example, the Z1 zone (grey) mainly consists of Ti and Mo while there are more O exists in the Z2 (dark) zone except for Ti and Mo. This result suggests that oxides, such as TiO_2 and MoO_3, are existed in the Z2 [37], which is caused by the squeezing and scraping between the alloy and the counter material during sliding. As for CP-Ti and Ti64 alloys, similar results were observed, e.g. TiO_2 and TiO_2-Al_2O_3 oxides are presented in the dark area (Fig. 8(e) Z3 and (f) Z4). Therefore, it is fair to assume that the abrasion and adhesion wear mechanism occurs for all alloys during tribocorrosion and pure mechanical wear.

3.4. *Synergy between corrosion and wear*

Calculations exemplifying the synergistic effect between wear and corrosion are shown in Fig. 9. It can be found in Fig. 9(b) that the wear increment rate due to the corrosion (4.7715 mm/yr) of Ti-16Mo alloy is s about 40% of pure mechanical wear rate (11.78 mm/yr), meaning the corrosion can greatly accelerate the wear loss. During sliding, a passive film formed on the surface is removed by severe mechanical forces. Then, a fresh unoxidized surface is exposed to a corrosive solution. This type of surface has high electrochemical activity, which will lead to the alloys dissolution and hence accelerate the wear loss. In addition, as Fig. 9(c) shown, corrosion rate enhances about 100 times from 0.00009 mm/yr to 0.00851 mm/yr under tribocorrosion condition. Plastic deformation is inevitable within the wear track under tribocorrosion conditions due to the continuing sliding action. This will induce lots of defect points, such as cracks and dislocations, which can act as the corrosion location, and hence accelerate the corrosion. Comparing with Fig. 9(a), (b), and (c), it can be found the total of pure mechanical wear and the pure corrosion rate is nearly same with the pure mechanical wear rate, while the total of wear and corrosion increment is nearly same with the wear rate increment. This result indicates that all the three alloys deterioration was mainly controlled by pure mechanical wear and corrosion-induced wear.

Comparing material loss of Ti-16Mo, CP Ti, and Ti64 in Fig. 9, it can be found that the Ti-16Mo alloy has the lowest materials loss, which can be ascribed to the following aspects: (1) the structural, component, and stability of the oxide film; and (2)

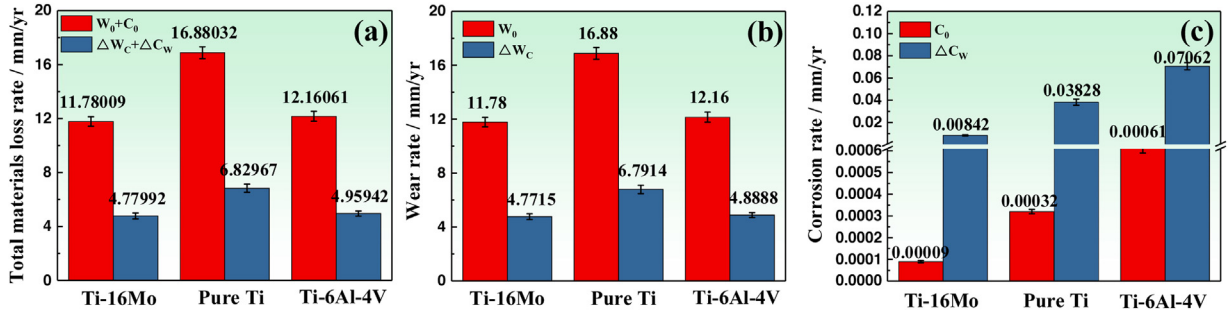

Fig. 9 – Synergistic contributions of wear and corrosion of Ti-16Mo, as-cast CP-Ti and Ti64 alloys in PBS solution at 37 ± 0.5 °C: (a) a total of pure mechanical wear and pure corrosion rate, and wear and corrosion increment, respectively; (b) pure mechanical wear rate and wear rate increment due to the corrosion; (c) pure corrosion rate and corrosion increment rate due to the wear.

high hardness. The addition of Mo to Ti makes the compact TiO_2-MoO_3 passive film formed, which can improve the corrosion resistance [22,38,39]. Additionally, Mo is a nobler element than Ti. When the corrosion occurs, the Mo elements can be dissolved preferentially until the formation of a passive oxide surface. For Ti64 alloy, there are lots of anion vacancies in the passive film due to the existence of V [40,41], which can reduce the stability of passive film and hence lower the corrosion resistance. Furthermore, higher hardness also can enhance the wear resistance of the alloys. Ti-16Mo alloy exhibits the highest hardness (Fig. 1(b)), and hence the alloy has a minimum damaged surface [42]. As a result, the Ti-16Mo alloy exhibits the lowest materials loss.

4. Conclusions

(1) The corrosion and wear accelerate each other significantly, and the corrosion rate and wear rate increase about 100 times and 40% under tribocorrosion, respectively.
(2) The materials loss of Ti-16Mo alloy is mainly due to pure mechanical wear and corrosion-induced wear. The wear mechanism of Ti-16Mo alloy is dominated by a combination of abrasion and adhesion.
(3) The total materials loss of Ti-16Mo alloy is 16.56001 mm/yr, which is lower than both as-cast CP-Ti (23.70999 mm/yr) and Ti64 alloys (17.12003 mm/yr). This makes Ti-16Mo alloy become a promising candidate for orthopedics implant applications.

Conflict of interest

The authors declare no conflicts of interest.

Data availability

The data that support the findings of this study are available from the corresponding authors on reasonable request.

Acknowledgments

This research work is supported by the National Natural Science Foundation of China (51922004, 51874037), State Key Lab of Advanced Metals and Materials, University of Science and Technology Beijing (2019-Z14) and Fundamental Research Funds for the Central Universities (FRF-TP-19005C1Z). Chaozong Liu acknowledges the support from the European Commission via the H2020 MSCA RISE BAMOS programme (734156). Wei Xu acknowledges the support from the China Scholarship Council (CSC) for a CSC Ph.D. scholarship (201906460106).

REFERENCES

[1] Wise DL, Trantolo DJ, Altobelli DE, Yaszemsk MJ, Grasser JD. Human biomaterials applications. Totowa, NJ: Humana Press; 1996.
[2] Yaszemsk MJ, Trantolo DJ, Lewandrowski KU, Hasirci V, Altobelli DE, Wise DL. Biomaterials in orthopedics. New York, NY: Marcel Dekker Inc.; 2004.
[3] Xu W, Lu X, Tian JJ, Huang C, Chen M, Yan Y, et al. Microstructure, wear resistance, and corrosion performance of Ti35Zr28Nb alloy fabricated by powder metallurgy for orthopedic applications. J Mater Sci Technol 2020;41:191–8.
[4] Geetha M, Singh AK, Asokamani R, Gogia AK. Ti-based biomaterials, the ultimate choice for orthopedic implants-A review. Prog Mater Sci 2009;54:397–425.
[5] Xu W, Xiao SQ, Lu X, Chen G, Liu CC, Qu XH. Fabrication of commercial pure Ti by selective laser melting using hydride-dehydride titanium powders treated by ball milling. J Mater Sci Technol 2019;35:322–7.
[6] Xu W, Lu X, Wang LN, Shi ZM, Lv SM, Ma Q, et al. Mechanical properties, in vitro corrosion resistance and biocompatibility of metal injection molded Ti-12Mo alloy for dental applications. J Mech Behav Biomed Mater 2018;88:534–47.
[7] Costa BC, Tokuhara CK, Rocha LA, Oliveira RC, Lisboa-Filho PN, Pessoa JC. Vanadium ionic species from degradation of Ti-6Al-4V metallic implants: in vitro cytotoxicity and speciation evaluation. Mater. Sci. Eng. C 2019;96:730–9.
[8] Aksakal B, Yildirim OS, Gul H. Metallurgical failure analysis of various implant materials used in orthopedic applications. J. Fail. Anal. Prev 2004;4:17–23.

[9] Ho WF, Ju CP, Lin JC. Structure and properties of cast binary Ti-Mo alloys. Biomaterials 1999;20:2115–22.
[10] Xu W, Liu Z, Lu X, Tian JJ, Chen G, Liu BW, et al. Porous Ti-10Mo alloy fabricated by powder metallurgy for promoting bone regeneration. Sci. China Mater 2019;62:1053–64.
[11] Disegi J. Wrought Titanium-15% molybdenum implant material. 2nd ed. SYNTHES® Instruments and Implants; 2009. April.
[12] ATI 15Mo™ Titanium alloy technical data sheet, ATI Allvac, Monroe, NC.
[13] Jablokov VR, Nutt MJ, Richelsoph ME, Freese HL. The application of Ti-15Mo beta titanium alloy in high strength structural orthopedic applications. J ASTM Int 2005;2:1–8.
[14] Xu W, Hou CJ, Mao YX, Yang L, Tamaddon M, Zhang JL, et al. Design and development of Ti-10Mo-xCu alloy fabricated by powder metallurgy for biomedical application. Bioact Mater 2020;5(3):659–66.
[15] Xu W, Chen M, Lu X, Zhang DW, Singh HP, Yu JS, et al. Effect of Mo content on corrosion and tribocorrosion behaviours of Ti-Mo orthopaedic alloys fabricated by powder metallurgy. Corros Sci 2020;168:108557.
[16] Oliveira NTC, Guastaldi AC. Electrochemical stability and corrosion resistance of Ti-Mo alloys for biomedical applications. Acta Biomater 2009;5:399–405.
[17] Chen YY, Xu LJ, Liu ZG, Kong FT, Chen ZY. Microstructures and properties of titanium alloys Ti-Mo for dental use. Trans Nonferrous Met Soc China 2006;16:s824–8.
[18] Marino CEB, Mascaro LH. EIS characterization of a Ti-dental implant in artificial saliva media: dissolution process of the oxide barrier. J Electroanal Chem (Lausanne) 2004;568:115–20.
[19] Yan Y, Neville A, Dowson D. Biotribocorrosion-an appraisal of the time dependence of wear and corrosion interactions: I. The role of corrosion. J Phys D Appl Phys 2006;39:3200–5.
[20] Kunčická L, Kocich R, Lowe TC. Advances in metals and alloys for joint replacement. Prog Mater Sci 2017;88:232–80.
[21] Hussein M, Mohammed A, Al-Aqeeli N. Wear characteristics of metallic biomaterials: a review. Materials 2015;8:2749–68.
[22] Xu W, Lu X, Zhang B, Liu CC, Lv SM, Yang SD, et al. Effects of porosity on mechanical properties and corrosion resistance of PM-fabricated porous Ti-10Mo alloy. Metals 2018;8:188–201.
[23] Lin YW, Lu X, Sun B, Liu CC, Qu XH. Microstructure and mechanical properties of Ti-Mo alloys by powder metallurgy process. Rare Metal. Mater. Eng 2017;46:1387–92.
[24] Xu W, Li M, Wen CE, Lv SM, Liu CC, Lu X, et al. The mechanical properties and in vitro biocompatibility of pm-fabricated Ti-28Nb-35.4Zr alloy for orthopedic implant applications. Materials 2018;11:531–43.
[25] Xu W, Tian JJ, Liu Z, Lu X, Hayat MD, Huang C, et al. Novel porous Ti35Zr28Nb scaffolds fabricated by powder metallurgy with excellent osteointegration ability for bone-tissue engineering applications. Mater. Sci. Eng. C 2019;105:110015.
[26] Xu W, Lu X, Hayat MD, Tian JJ, Huang C, Chen M, et al. Fabrication and properties of newly developed Ti35Zr28Nb scaffolds fabricated by powder metallurgy for bone-tissue engineering. J. Mater. Res. Technol 2019;8:3696–704.
[27] ASTM G59-97. Standard test method for conducting potentiodynamic polarization resistance measurements. West Conshohocken, PA: ASTM International; 2014.
[28] ASTM E384-11. Standard test method for Knoop and vickers hardness of materials. West Conshohocken, PA: ASTM International; 2011.
[29] ASTM G119-09. Standard guide for determining synergism between wear and corrosion. West Conshohocken, PA: ASTM International; 2016.
[30] Lu X, Sun B, Zhao TF, Wang LN, Liu CC, Qu XH. Microstructure and mechanical properties of spark plasma sintered Ti-Mo alloys for dental applications. Int J Min Met Mater 2014;21:479–86.
[31] Pina VG, Amigó V, Muñoz AI. Microstructural, electrochemical and tribo-electrochemical characterisation of titanium-copper biomedical alloys. Corros Sci 2016;109:115–25.
[32] Doni Z, Alves AC, Toptan F, Gomes JR, Ramalho A, Buciumeanu M, et al. Dry sliding and tribocorrosion behaviour of hot pressed CoCrMo biomedical alloy as compared with the cast CoCrMo and Ti6Al4V alloys. Mater Des 2013;52:47–57.
[33] Chen J, Yan FY, Chen BB, Wang JZ. Assessing the tribocorrosion performance of Ti-6Al-4V, 316 stainless steel and Monel K500 alloys in artificial seawater. Mater Corros 2013;64:394–401.
[34] Doni Z, Alves AC, Toptan F, Rocha LA, Buciumeanu M. Tribocorrosion behavior of hot pressed CoCrMo-HAP biocomposites. Tribol Int 2015;91:221–7.
[35] Zhang BB, Wang JZ, Yan FY. Load-dependent tribocorrosion behaviour of nickel-aluminium bronze in artificial seawater. Corros Sci 2018;131:252–63.
[36] Yan C, Zeng QF, Xu YT, He WJ. Microstructure, phase and tribocorrosion behavior of 60NiTi alloy. Appl Surf Sci 2019;498:143838.
[37] Yetim AF. Investigation of wear behavior of titanium oxide films, produced by anodic oxidation, on commercially pure titanium in vacuum conditions. Surf Coat Tech 2010;205:1757–63.
[38] Zhou YL, Luo DM. Corrosion behavior of Ti-Mo alloys cold rolled and heat treated. J Alloys Compd 2011;509:6267–72.
[39] Oliveira NTC, Guastaldi AC. Electrochemical behavior of Ti-Mo alloys applied as biomaterial. Corros Sci 2008;50:431–40.
[40] Niu WJ, Bai CG, Qiu GB, Wang Q. Processing and properties of porous titanium using space holder technique. Mater Sci Eng C 2009;506:148–51.
[41] Metikos-Hukovic M, Kwokal A, Piljac J. The influence of niobium and vanadium on passivity of titanium-based implants in physiological solution. Biomaterials 2003;24:3765–75.
[42] Movassagh-Alanagh F, Abdollah-Zadeh A, Aliofkhazraei M, Abedi M. Improving the wear and corrosion resistance of Ti-6Al-4V alloy by deposition of TiSiN nanocomposite coating with pulsed-DC PACVD. Wear 2017;390-391:93–103.